Available online at www.sciencedirect.com
ScienceDirect
Physics of the Earth and Planetary Interiors 159 (2006) 234–246
PHYSICS OF THE EARTH AND PLANETARY INTERIORS
www.elsevier.com/locate/pepi

Tradeoffs in chemical and thermal variations in the post-perovskite phase transition: Mixed phase regions in the deep lower mantle?

Frank J. Spera [a,b,*], David A. Yuen [c], Grace Giles [a]

[a] *Department of Earth Science, University of California, Santa Barbara, CA 93106, United States*
[b] *Institute for Crustal Studies, University of California, Santa Barbara, CA 93106, United States*
[c] *Department of Geology and Geophysics and Minnesota Supercomputer Institute, University of Minnesota, Minneapolis, MN 55455, United States*

Received 12 April 2006; received in revised form 7 July 2006; accepted 26 July 2006

Abstract

The discovery of a phase transition in Mg-rich perovskite (Pv) to a post-perovskite (pPv) phase at lower mantle depths and its relationship to D″, lower mantle heterogeneity and iron content prompted an investigation of the relative importance of lower mantle compositional and temperature fluctuations in creating topographic undulations on mixed phase regions. Above the transition, Mg-rich Pv makes up ∼70% by mass of the lower mantle. Using results from experimental phase equilibria, first-principles computations and empirical scaling relations for Fe^{2+}–Mg mixing in silicates, a preliminary thermodynamic model for the Pv to pPv phase transition in the divariant system $MgSiO_3$–$FeSiO_3$ is developed. Complexities associated with components Fe_2O_3 and Al_2O_3 and other phases (Ca-Pv, magnesiowustite) are neglected. The model predicts phase transition pressures are sensitive to the $FeSiO_3$ content of perovskite (∼ −1.5 GPa per 1 mol% $FeSiO_3$). This leads to considerable topography along the top boundary of the mixed phase region. The Clapeyron slope for the Pv → pPv transition at $X_{FeSiO_3} = 0.1$ is +11 MPa/K about 20% higher than for pure Mg-Pv. Increasing bulk concentration of iron elevates the mixed (two-phase) layer above the core–mantle boundary (CMB); increasing temperature acts to push the mixed layer deeper in the lower mantle perhaps into the D″ thermal-compositional boundary layer resting upon the CMB. For various lower mantle geotherms and CMB temperatures, a single mixed layer of thickness ∼300 km lies within the bottom 40% of the lower mantle. For low iron contents ($X_{FeSiO3} \sim 5$ mol% or less), two (perched) mixed phase layers are found. This is the divariant analog to the univariant double-crosser of Hernlund et al., 2005 [Hernlund, J., Thomas, C., Tackley, P.J., 2005. A doubling of the post-perovskite phase boundary and structure of the Earth's lowermost mantle. Nature 434, 882–886.]. The hotter the mantle, the deeper the mixed phase layer; the more iron-rich the lower mantle, the shallower the mixed phase layer. In a younger and hotter Hadean Earth with interior temperatures everywhere 200–500 K warmer, pPv is not stable unless the lower mantle bulk composition is Fe-enriched compared to the present-day upper mantle. The interplay of temperature and Fe-content of the lower mantle has important implications for lower mantle dynamics.

Keywords: Tradeoffs in chemical variations; Tradeoffs in thermal variations; Post-perovskite phase transition; Mixed phase regions; Deep lower mantle

1. Introduction

The discovery of a phase transition in Mg-perovskite to a higher pressure post-perovskite polymorph at lower mantle depths near the core-mantle boundary (CMB)

* Corresponding author. Tel.: +1 8058934880; fax: +1 8058932314.
E-mail address: spera@geol.ucsb.edu (F.J. Spera).

0031-9201/$ – see front matter © 2006 Elsevier B.V. All rights reserved.
doi:10.1016/j.pepi.2006.07.007

has rekindled interest in the nature of seismic layer D″ and the composition, mineral constitution and magnitude of heterogeneity of the lower mantle (Hirose et al., 2006). Direct evidence for a phase transition from Mg-rich perovskite (Pv) to a new post-perovskite phase (pPv) comes from both experiments, quantum mechanical calculations and indirectly from seismologists concerned with the velocity structure and anisotropy in the lower mantle and seismic layer D″ (Murakami et al., 2004; Shim et al., 2004; Iitaka et al., 2004; Tsuchiya et al., 2004a; Tsuchiya et al., 2004b; Oganov and Ono, 2004; Sidorin et al., 1998; Sidorin et al., 1999). The lower half of the lower mantle which extends from 0 km to 1100 km above the CMB and includes seismic layer D″ is of special interest because of possible differences in bulk composition between the bottom part of the lower mantle and overlying mantle (Van der Hilst and Karason, 1999; Kellogg et al., 1999; Boyet and Carlson, 2005; Nakagawa and Tackley, 2004). A phase transition is pertinent to understanding seismic layer D″ (∼0–200 km above CMB) as well as the composition and dynamics of the lower mantle. Seismologically on a global basis, D″ exhibits a complex structure with variable thickness (150–300 km) and strong seismic anisotropy. A very thin layer in which seismic velocities drop by ∼10% at some locations may indicate patchy melting at the bottom of D″ along the CMB (Williams and Garnero, 1996; Garnero et al., 2004) or may be related to a very iron rich silicate region (Mao et al., 2006). Seismic studies reveal significant small-scale topography on the core-mantle boundary itself (Earle and Shearer, 1997).

A variety of mechanisms have been proposed to account for the structure of D″ (Jellinek and Manga, 2004). D″ could represent a thermal boundary layer at the CMB that becomes unstable on a geologic time scale, releasing upwelling plumes of hot material (Yuen and Peltier, 1980; Olson et al., 1987). Subducted slabs, or portions thereof may come to rest at the base of the mantle and hence D″ could represent a slab graveyard. It has also been suggested that the CMB may represent a compositionally distinct reaction zone between the Fe-rich molten core and the silicate lower mantle (Jeanloz and Knittle, 1989). The variability of velocity gradients and thicknesses within D″ (Lay et al., 2004) makes it difficult to rule out conclusively any of these possibilities. Perhaps several are simultaneously important.

Seismologically observed complexity in the lower mantle reaches a maximum in its bottom 200–300 km, within D″ (Helmberger et al., 1998). Additional evidence suggests that structural and compositional heterogeneity is not solely confined to D″ but extends to ∼1000 km above the CMB, a region that encompasses the bottom 40% of the lower mantle (Van der Hilst et al., 1997; Grand et al., 1997). Differential travel-time residuals from core-refracted (PKP) waves are similarly consistent with the lack of spatially coherent structures in the lower mantle extending ∼1000 km above the CMB (Van der Hilst and Karason, 1999). Together, these observations suggest changes in bulk composition and degree of heterogeneity in the bottom 30–40% of the mantle ∼1000 km above the CMB. If a Pv + pPv mixed phase regions exist in the lower mantle, enhanced incoherent scattering might be expected. Kellogg et al. (1999) proposed a dynamical model of thermochemical convection in the lower mantle. They posit the existence of a variably thick layer intrinsically denser by about 4% by virtue of its composition (e.g., more iron rich) compared to the overlying mantle (Tedesco and Spera, 1991). Because this deep layer is hot, its net density is only slightly greater than adiabatic. This leads to substantial topography along its top due to the competing effects of temperature and compositional buoyancy, parameterized by the bulk Fe content of the lower mantle (e.g., molar Fe^{++}/Mg ratio). In particular, they proposed that the top of the region of enhanced seismic heterogeneity observed ∼1000–1300 km above the CMB is the manifestation of a boundary between an upper Fe-depleted MORB source region and a deeper Fe-enriched, intrinsically denser region below. Recently, it was suggested (Hernlund et al., 2005) that a pair of seismic discontinuities observed in some regions of D″ can be explained by the Pv to pPv phase transition as a result of a double-crossing of the phase boundary by the geotherm at two different depths. In the Hernlund et al. model, the effects of other chemical components such as $FeSiO_3$, Al_2O_3 or Fe_2O_3 on the Pv to pPv phase transition boundary are neglected, although they note that these components plus the latent heat associated with the phase transition would transform the phase discontinuity into a mixed phase region and create a more complex and heterogeneous structure. Although the univariant case is a good starting point, it is imperative to consider the effects of additional components, notably the dissolution of ferrous iron ($FeSiO_3$), on the Pv to pPv phase transition.

Here we focus upon the structure and thickness of a Pv + pPv ‘mixed layer’ or mixed phase region and explore the relative roles of compositional (Fe^{2+}/Mg ratio) and temperature fluctuations in creating topographic undulations at the top and bottom of the mixed phase region. We do this by developing a simple thermodynamic model based upon available experimental data and first-principles calculations and apply it to the Pv to pPv transition in the binary $FeSiO_3$–$MgSiO_3$ system. Because the effect of $FeSiO_3$ dissolution on the pressure

of the Pv to pPv polymorphic transition (Mao et al., 2004; Murakami et al., 2005) depends on the speculative bulk composition of the lower mantle (e. g., role of additional components and phases such as magnesiowustite (Murakami et al., 2005), we first discuss the relative roles of temperature and composition creating topography at the top of the mixed phase region. We consider cases $(\partial p/\partial X_{FeSiO_3})_T > 0$ and $(\partial p/\partial X_{FeSiO_3})_T < 0$ where p is the thermodynamic pressure of the phase transition. In the first case, positive temperature and composition fluctuations act in concert to displace the boundaries (top and bottom) of the mixed phase region whereas the opposite condition holds in the second case. Finally, we use available thermochemical information to develop a simple preliminary model of the Pv to pPv phase transition in the binary system $FeSiO_3$–$MgSiO_3$ assuming $FeSiO_3$ dissolution decreases the pressure of the Pv to pPv inversion (Mao et al., 2004; Stackhouse et al., 2005) and more fully explore the convective dynamical consequences of this scenario (Matyska and Yuen, 2005; Nakagawa and Tackley, 2006). This newly discovered phase transition can wield significant influence on the dynamics of D″ and the lower part of the lower mantle via the effects of combined temperature and compositional fluctuations and may additionally provide valuable constraints on the temperature and composition of the Earth's lower mantle.

2. Relative effects of temperature and composition on phase boundary height and topography

Topographic undulations on the univariant phase transition Mg-Pv to Mg-pPv can be significant from temperature, since the Clapeyron slope is large, close to 10 MPa/K (Tsuchiya et al., 2004a,b) for the transition. Temperature excursions of 100 K and 500 K give rise to 17 km and 85 km topographic deflections of the boundary, respectively. Traditionally, undulations of phase boundaries have been attributed strictly to thermal perturbations associated with erupting plumes (Schubert et al., 1975). However, there is mounting evidence that compositional variations, such as higher Fe^{2+}/Mg in the lower mantle compared to the upper mantle, play a significant role (Yuen et al., 1993; Ishii and Tromp, 1999; Trampert et al., 2004). It is timely to investigate the possibility that phase boundary undulations arise due to variations in Fe^{2+}/Mg and to study the role of composition on the Pv → pPv phase transition in deep mantle flow.

We examine several possible situations as depicted in Fig. 1. Consider the influence of temperature (δT) and compositional (δX) fluctuations on the height of the mixed-phase boundary ξ in a two-component system (e.g., $MgSiO_3$–$FeSiO_3$). The boundary could represent the top or bottom of a mixed (two-phase) phase layer. δT and δX are taken as positive quantities and without loss of generality we can focus on the top of the boundary. δX represents a fluctuation in the fraction of some component such as Al_2O_3, Fe_2O_3 or $FeSiO_3$ that sensibly affects the inversion pressure for the polymorphic transformation Pv → pPv. In a later section we focus upon component $FeSiO_3$, although the analysis here is general and can be applied to other components that dissolve in Mg-perovskite. Topographic undulations are related to the magnitude of δp, the change in the phase transition pressure (assumed hydrostatic) decomposed according to:

$$\delta p = \left(\frac{\partial p}{\partial T}\right)_X \delta T + \left(\frac{\partial p}{\partial X}\right)_T \delta X \quad (1)$$

The first partial derivative on the RHS of Eq. (1) is the Clapeyron slope for the Pv to pPv post-transition, ~8–10 MPa/K for pure Mg-Pv. This is larger and opposite in sign of the Clapeyron slope of the γ-spinel to perovskite transition of −3 MPa/K (~670 km depth) and indicates that temperature effects alone can be significant. The second partial derivative on the RHS of Eq. (1) can be positive or negative depending on the component under consideration. For Fe_2O_3, a post-perovskite phase with a $CaIrO_3$-type *Cmcm* structure is stable above 30 GPa at 1000 K with a positive Clapeyron slope of 4.6 MPa/K (Ono et al., 2005). This implies that $(\partial p/\partial X^{Pv}_{Fe_2O_3})_T$ is negative. For the charge coupled substitution [MgSi] ⇒ [AlAl] dissolution of 6.5 mol% Al_2O_3 in Mg-Pv increases the transition pressure by ~7 GPa at 0 K based on first-principles calculations (Akber-Knutson et al., 2005), That is, $(\partial p/\partial X^{Pv}_{Al_2O_3})_T$ is positive. In contrast, laboratory experiments (Mao et al., 2004) and *ab initio* calculations (Stackhouse et al., 2005) suggest that $(\partial p/\partial X^{Pv}_{FeSiO_3})_T$ is negative in the system $MgSiO_3$–$FeSiO_3$ although in pyrolitic bulk composition where additional phases such as magnesiowustite and Ca-perovskite are present the situation may be more complex (Murakami et al., 2005; see also Hirose et al., 2006). Fig. 1a (upper panel) portrays the situation when thermal buoyancy dominates over compositional buoyancy. If the effect of dissolution of a component is to increase the transformation pressure ($\partial p/\partial X > 0$), then temperature and composition act in concert and the phase boundary is depressed. If the presence of a component has the opposite effect (i.e., $\partial p/\partial X < 0$), then the phase boundary is depressed but less so than previous case since composition acts counter to the temperature pertur-

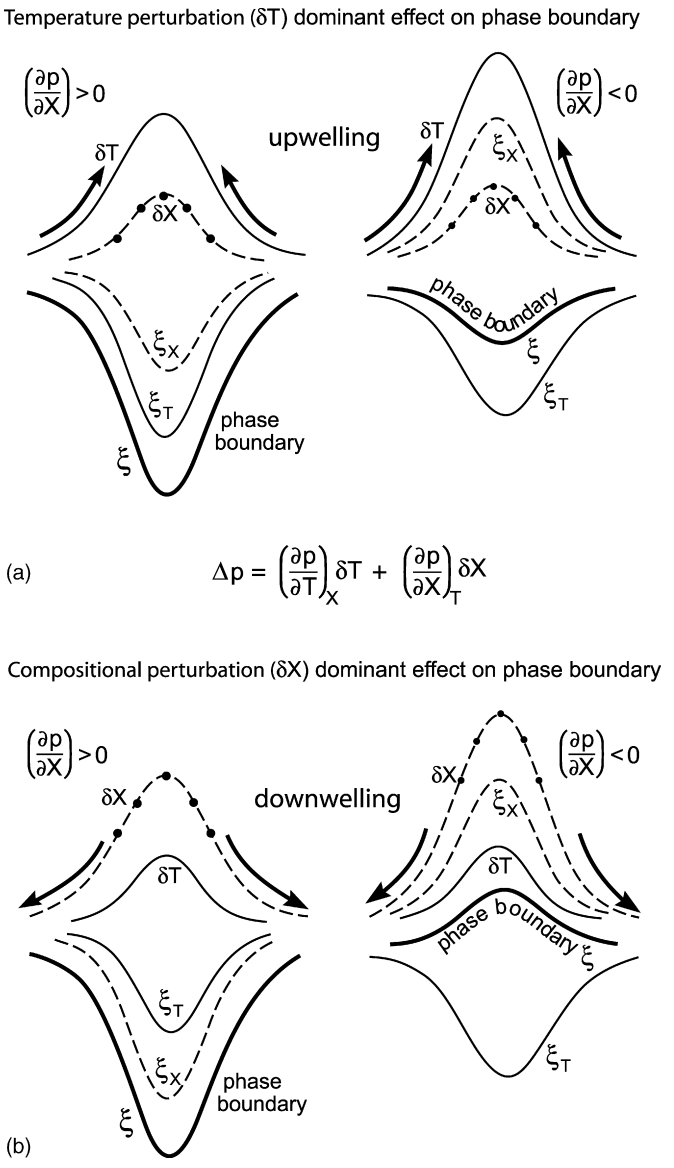

Fig. 1. Stability diagram showing the effects of fluctuations in temperature (δT) and composition (δX_{FeSiO_3}) on the topography of the phase boundary (i.e., top or bottom of mixed phase region). Upper panel shows case where thermal perturbations are dominant. This leads to upwelling lower mantle. The phase boundary is depressed because the Clapeyron slope of the Pv → pPv is ∼+10 MPa/K. If the inversion pressure increases with increasing Fe then the boundary is further depressed. If the pressure–composition derivative is <0 then the phase boundary is less depressed. Lower panel shows case when fluctuations in composition Fe/Mg ratio dominate the local buoyancy. These are regions of downwelling. If the pressure–composition derivative is positive, the phase boundary is depressed. However, for negative $\partial p/\partial X$, the boundary may be elevated because increasing the Fe content lowers the phase transition pressure along an isotherm.

bation. Fig. 1b (lower panel) depicts the situation when compositional buoyancy dominates over thermal buoyancy. Again, two cases are distinguished. If $\partial p/\partial X > 0$, then because chemical buoyancy dominates, the phase boundary will be depressed. Reciprocally, if $\partial p/\partial X < 0$, then the phase boundary is elevated despite the opposing effects of thermal fluctuations.

For the specific case where the additional component is $FeSiO_3$, we can provide a more quantitative analysis. In this case, $(\partial p/\partial X^{Pv}_{FeSiO_3})_T$ is computed from thermodynamic analysis relevant to the analog mantle system $MgSiO_3$–$FeSiO_3$ (see below) and is of order −150 GPa or 1.5 GPa per mol% $FeSiO_3$ component dissolved in Mg-rich Pv. Note the opposite effects of

temperature (δT) and composition (δX_{Pv}) fluctuations on the height of the transition boundary. This case is analogous to the one depicted on the right-hand side of Fig. 1b (lower panel). From Eq. (1) we find that, $\delta T/\delta X \approx -150$ K/mol% $FeSiO_3$ in Pv. That is, a cold temperature fluctuation of -150 K is required to offset the decrease in transformation pressure due Fe-enrichment in Mg-rich perovskite by 1 mol%. Such a small variation in composition is easily obtainable in thermal-chemical convection (Hansen and Yuen, 1988).

Applying Eq. (1) to undulations at the top of the mixed-phase region reveals the potential importance of small variations in the Fe content (X_{FeSiO_3}) of Mg-rich perovskite. Imagine a location with $\delta T \sim +100$ K perhaps due to a local 'hot spot' on the CMB. For *pure* Mg-perovskite, this would *depress* the boundary of the mixed phase region by

$$\delta\xi = -(\rho g)^{-1}\left(\frac{\partial p}{\partial T}\right)_X \delta T \approx -20\,\text{km} \qquad (2)$$

where ρ is the lower mantle density and g, the local acceleration due to gravity. However, if this same thermal perturbation is associated with an increase in the iron content of Pv from $X^{Pv}_{FeSiO_3} = 0.10$ to $X^{Pv}_{FeSiO_3} = 0.15$ then the net effect *elevates* the boundary by roughly $\delta\xi = 110$ km.

From a dynamical point of view (Fig. 2), the presence of undulations at the top of a mixed layer provides a source of localized force in the momentum equation due to the density difference associated with the phase transition (Richter, 1973). There is now an additional coupling between the momentum equation and species conservation. The additional coupling arises from (1) chemically-induced buoyancy terms (composition and phase abundance) of localized nature in the momentum equation and (2) chemically-induced source terms in latent heat release (Pv → pPv is exothermic) in the energy equation. These two contributions will make the overall system more nonlinear than thermal convection with phase transitions in a one-component system. Previous work has been carried out for the garnet–spinel system at the 670 km discontinuity (Nakagawa and Tackley, 2004), although phase boundary undulations from multi-component compositional effects were not emphasized.

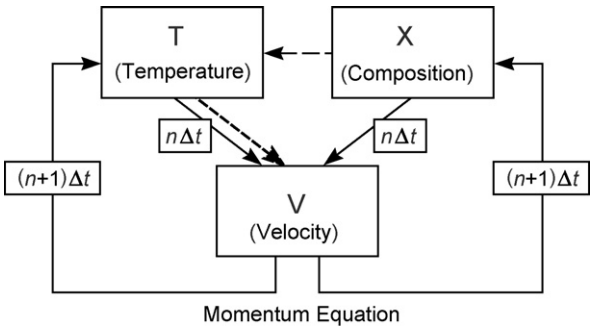

Fig. 2. Energy–momentum equation feedbacks in divariant mixed phase equilibria and mantle flow. Buoyancy is a function of bulk composition, phase abundance and temperature. Reaction liberates enthalpy, a heat source. Viscosity depends on phase abundance, temperature and pressure as does isobaric heat capacity and thermal conductivity.

3. Thermodynamic formulation

3.1. Binary component equilibria

It is of interest to calculate the Clapeyron slope and the pressure of the perovskite (Pv) to post-perovskite (pPv) phase transition for composition and temperature appropriate for the lower mantle. This is a complex problem because the effects of dissolution of Fe_2O_3, $FeSiO_3$ and Al_2O_3 on the stability of Mg-rich Pv and pPv phases, the role of additional phases (e.g., Ca-rich Pv and magnesiowustite) and uncertainties in the temperature and bulk composition in the lower mantle remain large. From the point of view of laboratory experiments, different pressure scales used by various workers to calibrate the Pv → pPv transition introduces additional uncertainty (see Hirose et al., 2006 for discussion). However, basic thermodynamic reasoning along with some estimates of thermochemical parameters enables one to establish a preliminary model for the dissolution of $FeSiO_3$ in coexisting Mg-rich perovskite and post-perovskite phases in the lower mantle. This is a simplified analog system that incorporates to first order the important effects of ferrous iron dissolution in Mg-Pv and is consistent with available experimental and theoretical constraints and the energetics of $FeSiO_3$–$MgSiO_3$ mixing in crystalline Fe–Mg silicates.

In a two-phase (Pv + pPv) binary component ($FeSiO_3$–$MgSiO_3$) crystalline solution, the conditions for equilibrium in the mixed phase region are:

$$\mu^{pv}_{FeSiO_3} = \mu^{ppv}_{FeSiO_3} \quad \text{and} \quad \mu^{pv}_{MgSiO_3} = \mu^{ppv}_{MgSiO_3} \qquad (3)$$

where μ^{α}_i represents the chemical potential of the ith component in phase alpha. Expanding the equilibrium condition enables one to explicitly link temperature (T), pressure (p) and the composition, expressed in terms of the mole fraction of $FeSiO_3$ component in co-existing Pv and pPv (Pitzer, 1995; Navrotsky, 1994). The phase is denoted by the superscript Pv or pPv. This model allows for non-ideal mixing of Fe^{2+} and Mg in both phases according to the strictly regular solution model formulation. That is, we allow for non-ideal Fe–Mg mixing in

both Pv and pPv. The expanded form of (1) is written:

$$\Delta H_{\mathrm{Fe}}(T) - T\Delta S_{\mathrm{Fe}}(T) + \int_{P_r}^{P} \Delta V_{\mathrm{Fe}}\mathrm{d}p + RT \ \ln\left(\frac{X_{\mathrm{Fe}}^{\mathrm{ppv}}}{X_{\mathrm{Fe}}^{\mathrm{pv}}}\right) + W_{\mathrm{ppv}}(1 - X_{\mathrm{Fe}}^{\mathrm{ppv}})^2 - W_{\mathrm{pv}}(1 - X_{\mathrm{Fe}}^{\mathrm{pv}})^2 = 0 \quad (4)$$

and

$$\Delta H_{\mathrm{Mg}}(T) - T\Delta S_{\mathrm{Mg}}(T) + \int_{P_r}^{P} \Delta V_{\mathrm{Mg}}\mathrm{d}p + RT \ \ln\left(\frac{1 - X_{\mathrm{Fe}}^{\mathrm{ppv}}}{1 - X_{\mathrm{Fe}}^{\mathrm{pv}}}\right) + W_{\mathrm{ppv}}(X_{\mathrm{Fe}}^{\mathrm{ppv}})^2 - W_{\mathrm{pv}}(X_{\mathrm{Fe}}^{\mathrm{pv}})^2 = 0 \quad (5)$$

where, for brevity, the subscript Fe or Mg is used to denote $FeSiO_3$ or $MgSiO_3$ component, respectively. The parameters W_{Pv} and W_{pPv} represent the Margules parameters that describe Fe–Mg mixing in Pv phase and pPv phase, respectively. For ideal mixing both W_{Pv} and W_{pPv} are identically zero. In the strictly regular solution model, W_{Pv} and W_{pPv} are constants, independent of temperature, pressure and composition. The Margules parameters relate to the activity coefficients according to $RT \ln \gamma_{\mathrm{FeSiO_3}}^{\mathrm{Pv}} = W_{\mathrm{Pv}}(1 - X_{\mathrm{FeSiO_3}}^{\mathrm{Pv}})^2$. Similar expressions follow for $MgSiO_3$ component in both Pv and pPv.

In Eqs. (4) and (5), $\Delta H(T)$, $\Delta S(T)$ and ΔV (p, T) represent the enthalpy, entropy and volume change for the reactions $FeSiO_3$ (Pv) → $FeSiO_3$ (pPv) and $MgSiO_3$ (Pv) → $MgSiO_3$ (pPv), $X_{\mathrm{Fe}}^{\mathrm{pv}}$ denotes the mole fraction of $FeSiO_3$ in perovskite, $X_{\mathrm{Fe}}^{\mathrm{ppv}}$ is the mole fraction of $FeSiO_3$ in post-perovskite and the subscripts on the enthalpy, entropy and volume change refer to the Pv → pPv transition for Fe and Mg end-member reactions, respectively. Because we used high temperature data to calibrate these equilibria, we assume ΔC_p for both reactions is zero in the temperature interval of interest (approximately 2000–4000 K) consistent with saturation of vibrational states at high temperature. This neglects heat capacity effects associated with different spin states for Fe that are most likely small compared to other uncertainties (Badro et al., 2003, 2004; Brodholt and Dobson, 2005). If we further assume that, in the pressure range of interest, the volume *change* for the end-member reactions are constant, then Eqs. (4) and (5) represent two equations in the four unknowns T, p, $X_{\mathrm{Fe}}^{\mathrm{pv}}$ and $X_{\mathrm{Fe}}^{\mathrm{ppv}}$ given the thermodynamic parameters that include the (constant) enthalpy, entropy and volume change of each end-member reaction as well as two regular solution parameters (W_{Pv} and W_{pPv}) to describe Fe^{2+}–Mg mixing. Navrotsky (1994) has noted an empirical correlation between end-member volume mismatch and the Margules parameter (W) for a number of crystalline silicate and oxide systems and we exploit this scaling relationship in the thermodynamic analysis.

In Table 1, the set of derived thermodynamic parameters are presented for the governing equilibria expressed in Eq. (3). We emphasize that the constraints are few and the thermochemical model is preliminary. The uncertainties are estimated from experimental uncertainties on pressure and temperature cited in the original references. As more data become available, it should be possible to incorporate the effects of Fe_2O_3, Al_2O_3 and CaO on the relevant polyphase equilibria and to improve the crystalline solution model and hence predictions by Gibbs energy minimization of phase equilibria.

3.2. *p–X and T–X sections*

In Fig. 3, a schematic p–X section is shown. In order to evaluate the dynamics and stability of the mixed layer near the base of the mantle, it is important to weigh the effects of temperature and composition, notably X_{Fe}, the mole fraction of $FeSiO_3$ component in coexisting Pv and pPv, on the convective dynamics of the mixed layer region. In order to do this, the derivatives $(\partial p/\partial X_{\mathrm{Fe}}^{\mathrm{ppv}})_T$

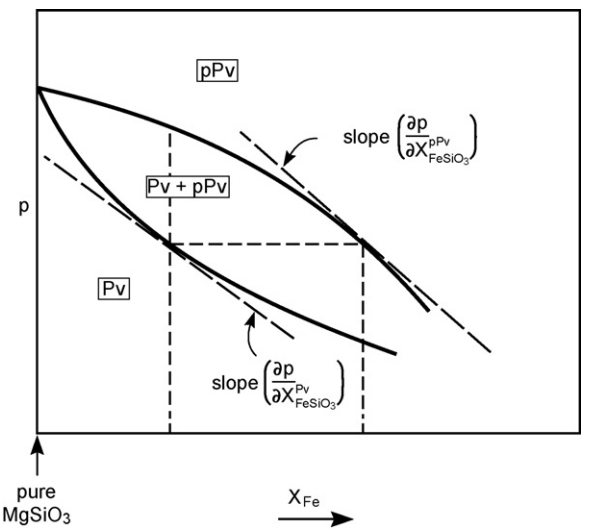

Fig. 3. Schematic isothermal pressure–Composition (P–X) section illustrating divariant phase relations in system $MgSiO_3$–$FeSiO_3$. At some pressure indicated by the dashed horizontal line and for any bulk composition between the vertical dashed lines, two phases (Pv + pPv) are present. The abundance depends on the bulk composition. The pressure–composition derivative defining the top of a mixed phase region (at low pressure) is less steep than that for the Pv-out boundary. These thermodynamic derivatives are useful in estimating mixed phase region topography and are calculated from data in Table 1 (see text).

Table 1

Reaction	ΔH (J/mol)	ΔS (J/K mol)	ΔV (m^3/mol)		
$MgSiO_3$ (Pv) ⇒ $MgSiO_3$ (pPv)	27427 ± 2500	−2.566 ± 0.2	$(-2.779 \pm 0.2) \times 10^{-7}$	Fe–Mg Margules parameter for Pv (J/mol) – W^{Pv}	12343
$FeSiO_3$ (Pv) ⇒ $FeSiO_3$ (pPv)	54000 ± 4500	−3.108 ± 0.36	$(-8 \pm 3) \times 10^{-7}$	Fe–Mg Margules parameter for pPv (J/mol) –W^{pPv}	16068

and $(\partial p/\partial X^{pv}_{Fe})_T$ are evaluated and the effects of composition on the transition pressure can be compared with thermal effects. The two derivatives are indicated schematically on Fig. 3. The derivatives are computed by differentiation of Eqs. (4) and (5) with respect to pressure at constant temperature to give:

$$\Delta V_{Fe} + A\left(\frac{\partial X^{pPv}_{Fe}}{\partial p}\right)_T - B\left(\frac{\partial X^{Pv}_{Fe}}{\partial p}\right)_T = 0 \quad (6)$$

and

$$\Delta V_{Mg} - C\left(\frac{\partial X^{pPv}_{Fe}}{\partial p}\right)_T + D\left(\frac{\partial X^{Pv}_{Fe}}{\partial p}\right)_T = 0 \quad (7)$$

where $A \equiv (RT/X^{pPv}_{Fe}) - 2W_{ppv}(1 - X^{pPv}_{Fe})$, $B \equiv (RT/X^{Pv}_{Fe}) - 2W_{pv}(1 - X^{Pv}_{Fe})$, $C \equiv (RT/1 - X^{pPv}_{Fe}) - 2W_{ppv}(1 - X^{pPv}_{Fe})$ and $D \equiv (RT/1 - X^{Pv}_{Fe}) - 2W_{pv}X^{Pv}_{Fe}$. Eqs. (6) and (7) represent two equations in the two unknown pressure-derivatives and may be solved to obtain the slopes of the phase transition loop curves $(\partial p/\partial X^{Pv}_{Fe})_T$ and $(\partial p/\partial X^{pPv}_{Fe})_T$. These derivatives, depicted schematically on Fig. 3, are written:

$$\left(\frac{\partial p}{\partial X^{pPv}_{Fe}}\right)_T = \frac{BC - AD}{D\Delta V_{Fe} + B\Delta V_{Mg}} \quad (8)$$

and

$$\left(\frac{\partial p}{\partial X^{Pv}_{Fe}}\right)_T = \frac{BC - AD}{C\Delta V_{Fe} + A\Delta V_{Mg}}. \quad (9)$$

Parameters to compute A, B, C and D are collected in Table 1.

Eq (9) was used in Eq. (1) to compare compositional and thermal effects on generation of topographic undulations at the top boundary of the mixed layer. There we showed that small variations of the bulk Fe^{2+}/Mg ratio in the simple two-phase mantle analog system $FeSiO_3$–$MgSiO_3$ induce considerable topography and structure to the mixed phase region. The modal abundance of Pv and pPv does not vary linearly with depth through the mixed phase region and might contribute to incoherent scattering of seismic waves. The variation of transformation pressure with composition from Eq. (9) is plotted in Fig. 4 as a function of the $FeSiO_3$ content of the Pv phase for the isotherms $T = 2500$ K, 3500 K and 4000 K. For $X^{Pv}_{FeSiO_3}$ in the range 0.05–0.20, the pressure-derivative varies from ∼1.6 GPa per 1 mol% $FeSiO_3$ to 0.7 GPa per 1 mol% $FeSiO_3$. Evidently, small variations in iron content of only a few mol% can be important in generating topography at the top (and bottom) of the mixed phase region. One mole percent increase in $FeSiO_3$ component dissolved in Mg-rich Pv has the same effect on mixed phase region topography as a temperature variation of ∼−150 K for bulk composition $X^{BC}_{FeSiO_3} = 0.05$.

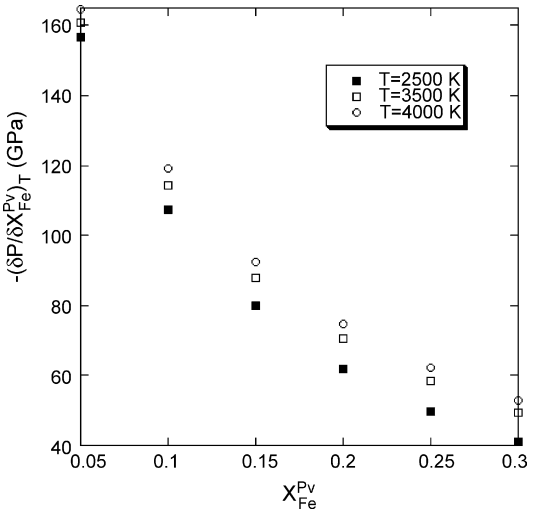

Fig. 4. The composition-derivative of the phase transition pressure in terms of the mole fraction of $FeSiO_3$ component dissolved in Mg-rich perovskite (Pv) vs. the mole fraction of $FeSiO_3$ component in Pv at $T = 2500$ K, 3500 K and 4000 K.

4. Results

Before embarking on detailed thermochemical convection studies, we can gain a useful first-order view using simple input functions. The location (i.e., the height above the CMB), thickness, phase compositions

and modal proportions in the mixed phase region may be estimated given a lower mantle geotherm and the bulk composition from the simplified (two phase-binary component) thermodynamic model. The molar Fe^{2+}/Mg ratio in the bulk composition or in a phase equals $X_{Fe}/(1-X_{Fe})$ where X_{Fe} is the mole fraction of $FeSiO_3$ in the bulk composition or in a phase (Pv or pPv). We first examine the isothermal case and then consider different lower mantle geotherms. For certain range of bulk compositions stacked mixed phase regions develop. This situation is similar to the "double-crosser" noted by Hernlund et al., 2005.

4.1. Location and thickness of mixed phase region: isothermal case

As an end member, we take an isothermal case and construct a series of isothermal *p–X* sections (Fig. 5). Comparison of the 2500 K, 3500 K and 4000 K isothermal sections indicates that for fixed bulk composition the transformation pressure for Pv → pPv increases as temperature increases. For example, at 2500 K, the inversion pressure at the top of the mixed layer is ~96 GPa (~720 km above CMB) for $X^{Pv}_{FeSiO_3} = 0.2$ whereas at 4000 K, p_{inv} is 110 GPa (~420 km above CMB).

The depth and thickness of the mixed phase region as a function of $X^{BC}_{FeSiO_3}$, the mole fraction of $FeSiO_3$ in the bulk composition, at different temperatures is sketched in Fig. 6. Pressure is related to height above the CMB from the PREM model (Dziewonski and Anderson, 1981). Examination of Fig. 6 reveals that a perched mixed phase region develops in the lower mantle in all cases. The depth and thickness of the mixed region depends on both temperature and lower mantle bulk composition (BC), parameterized by the mole fraction of $FeSiO_3$. For example, at 3500 K, the top of the mixed phase region increases from 372 km to 560 km above the CMB as the $Mg^{\#}$ ($Mg^{\#} \equiv 1 - X^{BC}_{FeSiO_3}$) decreases from 0.9 to 0.8. The thickness of the mixed phase region increases slightly from 167 km to 244 km for the same increase in X_{FeSiO3}. At 2500 K, the top of the mixed phase layer rises 720 km above the CMB and its thickness is 300 km for $Mg^{\#} = 0.8$. It is clear from Fig. 6 that small spatial variations in the $FeSiO_3$ content of the lower mantle potentially generate considerable topography at the top of the mixed layer. The mixed layer thickens as the bulk composition becomes more iron-rich and the thickness of the layer decreases for fixed bulk composition as the temperature increases. The mixed layer moves to greater heights above the CMB in response to lower temperatures and higher $X^{BC}_{FeSiO_3}$. Recall that the Fe-enriched layer hypothesized by Kellogg et al. (1999) extends from

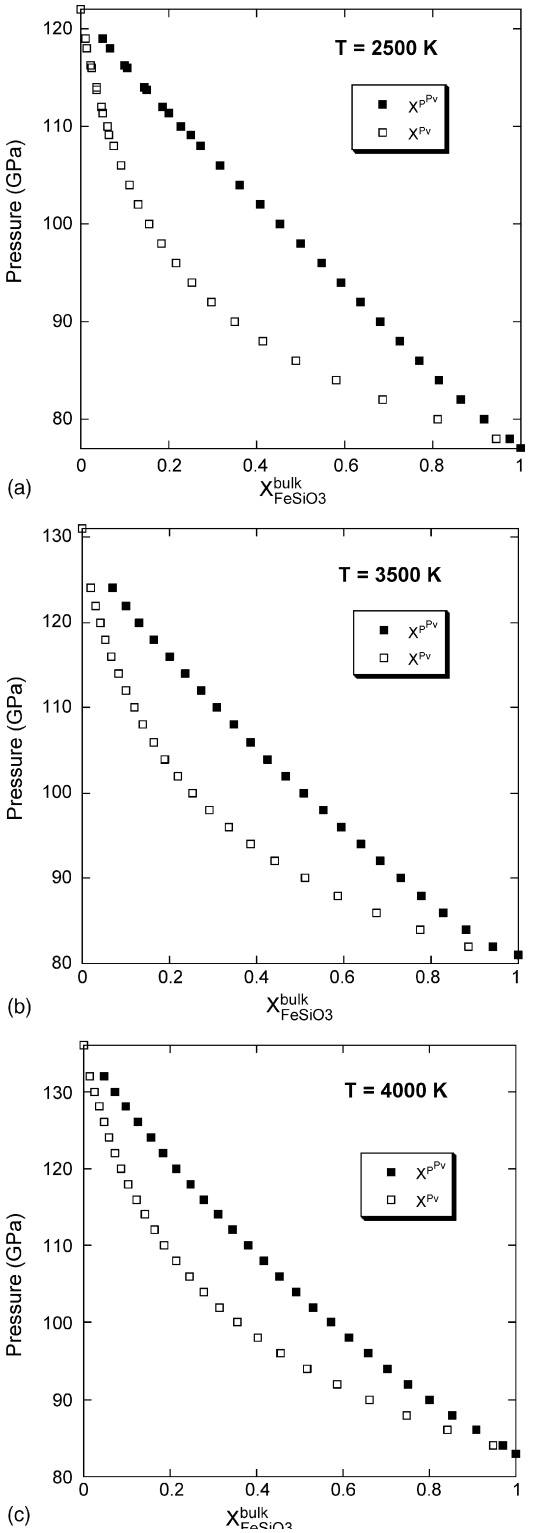

Fig. 5. Isothermal *P–X* sections showing the region of mixed phases as a function of *P*, *T* and bulk composition: (a) 2500 K; (b) 3500 K; (c) 4000 K.

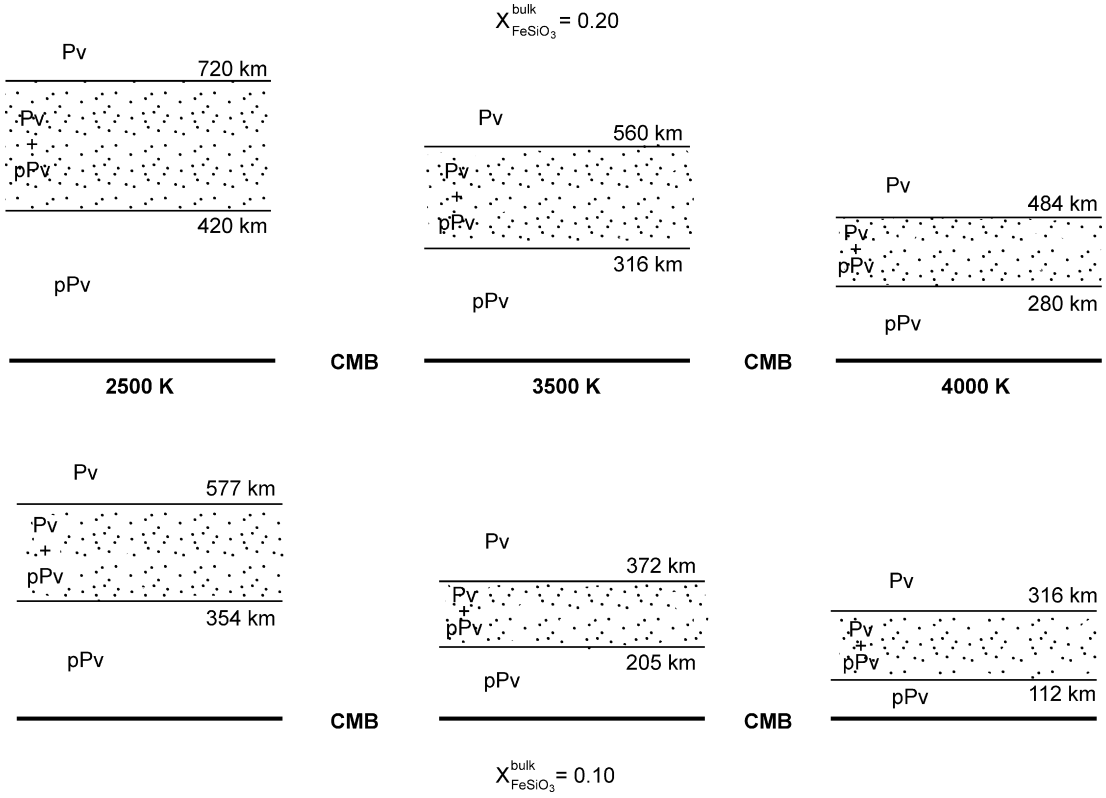

Fig. 6. Schematic depiction of the thickness and height above the CMB of the mixed (Pv + pPv) phase layer on the 2500 K, 3500 K and 4000 K isotherms for lower mantle bulk compositions of 0.1 and 0.2 mole fraction Fe/(Fe + Mg). The effect of increasing temperature at fixed bulk composition is to make the mixed phase layer thinner and deeper. The effect of increasing the iron content at fixed temperature is to make the layer shallower and thicker. The modal amount of pPv increases monotonically (but not linearly) with increasing depth.

the CMB to about 1000 km above the CMB. That height corresponds to the top of a mixed phase layer in Fe-enriched relatively cool mantle. For a very hot lower mantle ($T > 4000$ K) and low Fe content (<0.1), the mixed phase layer lies upon the CMB itself (Oganov and Ono, 2004).

The dependence of the inversion pressure on Fe content makes the Pv → pPv polymorphic reaction a potentially sensitive indicator of lower mantle temperature and especially lower mantle FeO content.

4.2. Location and thickness of mixed phase region for representative geotherms

To model more realistically the location and thickness of the mixed layer and discover the conditions that lead to multiple mixed layers (cf. the "double crosser" of (Hernlund et al., 2005)), we calculated the location and thickness of the mixed phase region for different bulk compositions and different families of mantle geotherms. The temperature at the CMB is set at 4100 K (Boehler, 2000; Alfe et al., 2002). We set the thickness of the thermal boundary layer defining D″ to be 190 km and show the position and thickness of the calculated mixed phase region along the 2400 K and 3400 K adiabats in Fig. 7. Geotherms are refracted across mixed phase region due to the exothermic nature of the Pv → pPv transition. The temperature change associated with the phase transition is $\Delta T = \Delta H/C_p \approx 290$ K (Table 1). The temperature gradient $\Delta H/h_{ML}C_p$ is added to the adiabatic gradient to give the geotherm within the mixed layer (h_{ML} is the mixed layer thickness and C_p is the isobaric specific heat capacity, $C_p \sim 1$ kJ/kg K).

The results show the existence of a perched mixed phase layer ~250 km thick with a top between 500 km to 735 km above the CMB depending on the assumed bulk composition and lower mantle geotherm (2400 K or 3400 K). The effect of increasing the molar Fe/(Fe + Mg) ratio is to raise the mean height of the mixed layer above the CMB for a fixed mantle adiabat. At fixed composition, a hot geotherm moves the perched mixed phase region deeper (closer to the CMB).

Seismic tomographic studies reveal that between ~400 km and 1200 km above the CMB the mantle

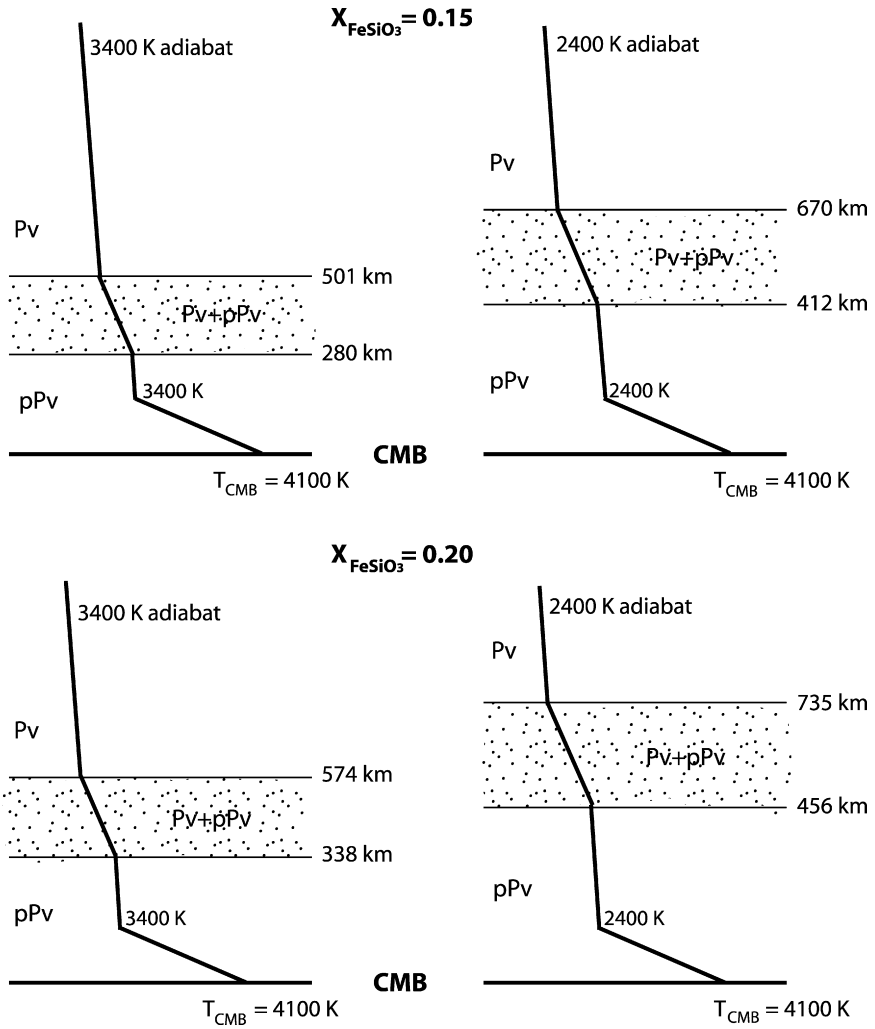

Fig. 7. Phase relations in the lower mantle for non-isothermal conditions. CMB temperature is 4400 K, thickness of D″ thermal boundary layer is 190 km. Hot (3400 K adiabat) and cold (2400 K adiabat) geotherms are shown. The adiabat outside the mixed phase region is 0.1 K/km in the lower mantle. In the mixed phase region, the geotherm becomes steeper due to the release of enthalpy for the exothermic reaction Pv → pPv using parameters of the thermochemical model in Table 1.

structure is heterogeneous and not consistent with well-mixed mantle (Van der Hilst et al., 1997). Additionally, the radial two-point correlation function for P-wave velocities (Puster and Jordan, 1997), a measure of the correlation between wavespeed anomalies at different depths, reaches a minimum in this region (Van der Hilst and Karason, 1999; Kennett, 1998). This same region (∼400–1100 km above the CMB) is characterized by enhanced scattering of short-period *PKP* elastic waves (Hedlin et al., 1997; Brana and Helffrich, 2004). Interestingly, it is in this same range of heights above the CMB (∼300–900 km) that the simple thermodynamic model presented here predicts the existence of mixed phase regions.

4.3. Conditions for doubly perched mixed phase layers

To study the conditions necessary for development of a pair of mixed phase layers (i.e., two distinct mixed layers separated by a single phase region, the divariant analog of the univariant 'double-crossers' of Hernlund and co-workers), the height above the CMB (h_{CMB}) and thickness of mixed phase region is plotted as function of the iron content ($X_{\mathrm{FeSiO_3}}$) of the lower mantle for two representative adiabats in Fig. 8. For the hot (3400 K) adiabat only a single layer develops at any bulk composition. The mixed layer rests on the CMB for $X_{\mathrm{FeSiO_3}} < 0.05$ and becomes progressively perched

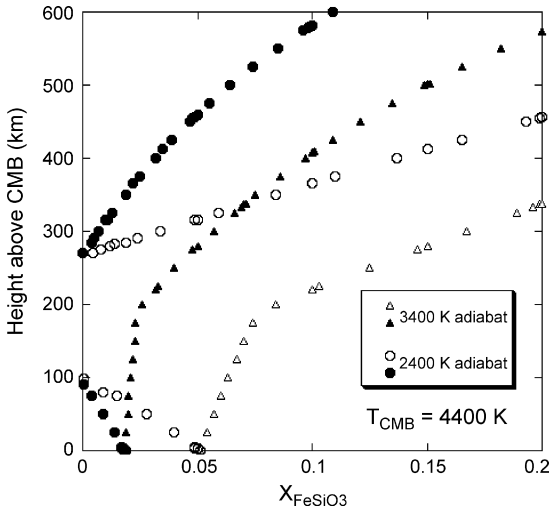

Fig. 8. Thickness and height above the CMB for the 2400 K and 3400 K adiabat with fixed CMB temperature of 4400 K as a function of the lower mantle bulk composition molar ratio Fe/Fe + Mg. In the 3400 adiabat case at $X_{FesiO_3} = 0.1$, the top and bottom of the mixed phase layers lies 400 km and 200 km above the CMB, respectively. For X_{FeSiO_3} less than ∼2 mol% there is no mixed layer and Pv is a stable at the CMB. For a cooler mantle (2400 K adiabat), two mixed phase regions can develop when Fe/Fe + Mg < 5 mol%. The top of the mixed phase region moves to substantially greater hights above the CMB as the iron content increases. For $X_{FeSiO_3} = 0.2$, the top of the mixed phase region for a cool mantle reaches 700–900 km above the CMB with a thickness approaching 500 km.

above the CMB as X_{FeSiO_3} increases. For example, for a lower mantle with $X_{FeSiO_3} > 0.10$, a mixed layer of thickness ∼120 km lies above a deep pPv layer essentially coincident with the D″ thermal boundary layer that rests on the CMB.

The situation is more interesting for the cold (2400 K) adiabat. In this case, an arrangement of double mixed layers is found for $X_{FeSiO_3} < 0.05$ such that a basal mixed layer resting on the CMB is separated from a second mixed phase layer by a ∼200 km pPv-only region. For these low iron content bulk compositions, the arrangement of phase regions is Pv → (Pv + pPv) → pPv → (Pv + pPv) with increasing depth starting in the middle part of the lower mantle. The cold adiabat case might be characteristic of the lower mantle under a subduction region. For example, in the Northern Pacific under Japan, one may expect more complexity in the lower mantle associated with multiple mixed phase regions. Although not explored in detail here, the structures that develop when temperature inversions occur along the geotherm due, for example from pinching off of hot diapirs (Brunet and Yuen, 2000) or the accumulation of detached cold Fe-depleted slabs can be quite complex and might lead to enhancement of scattering sites for seismic waves (Brana and Helffrich, 2004; Hedlin and Shearer, 2002; Nolet et al., 2006). The heterogeneity inferred by Van der Hilst and Karason (1999) from seismic data might be related to the presence of mixed phase regions in the lower part of the lower mantle. Regions with different scattering intensities in the deep mantle may reflect lateral differences in the subducting regions.

5. Conclusion

A preliminary thermodynamic model for the divariant ($MgSiO_3$–$FeSiO_3$) perovskite → post-perovskite phase transition for conditions relevant to the deep lower mantle has been developed based on laboratory and theoretical considerations. The model is simplified in that the effects of dissolved Al_2O_3 and Fe_2O_3 and the presence of additional phases (e.g., Ca-rich perovskite and magnesiowustite) are neglected (Ono et al., 2005; Akber-Knutson et al., 2005). Nevertheless, because Mg-rich perovskite accounts for ∼70% by mass of the lower mantle and because the dissolved $FeSiO_3$ content of Pv can be significant, the model has relevance to the Earth. For reasonable molar Fe/(Fe + Mg) ratios between ∼0.05–0.20 and typical lower mantle geotherms and CMB temperatures (3800–4400 K), we find that mixed phase regions of typical thickness ∼200–400 km lie perched above the CMB. The bottom of the mixed phase region typically lies 200–400 km above and the top at 450–700 km above the CMB, respectively. This is the same region of the lower mantle where seismic data suggests significant heterogeneity, anomalous scattering and higher iron content than the overlying upper part of the lower mantle. Accumulation of Mg-rich oceanic lithospheric slabs (low Fe) would tend to deepen and thin the mixed phase layer. For low Fe contents in cool mantle doubly perched mixed layers could develop. Subduction of significant volumes of Archean-Proterozoic banded iron formations (Brodholt and Dobson, 2005) leads to a shoaling and thickening of the perched mixed phase layer. In a hot lower mantle, the mixed phase zone essentially coincides with D″ unless very iron-rich. Further studies in the laboratory and from theory are needed to more fully explore spin effects in Fe, the role of other components (simultaneous dissolution of Fe_2O_3 and Al_2O_3) and the effects of including additional lower mantle phases such as magnesiowustite. Mapping the Pv → pPv phase transition in the lower mantle may be a useful technique for estimating simultaneously lower mantle temperature and composition (Fe content). Recently, new *ab initio* calculations of the athermal elastic constants of pure end-member $FeSiO_3$ have been presented

by Stackhouse et al. (2005). Their calculations are consistent with the lowering of the Pv to pPv transition pressure by incorporation of $FeSiO_3$ component as in our model, although the magnitude is somewhat smaller than that estimated here and has the effect of pushing the mixed phase layer deeper into the traditional D″ region. On the other hand, their estimate includes the simultaneous effects of 4 mol% Al_2O_3 dissolution and that will tend to increase the phase transition pressure. Hirose (2006) has presented a comparison of experimental and theoretical results on the Pv → pPv transition and attendant geophysical implications. Despite unresolved questions, it appears safe to conclude that the large seismic anomalies observed in the lower mantle and especially in D″ are ultimately related to the Pv to pPv phase transition. The strongly exothermic nature of the phase transition promotes the growth of thermally driven instability that may or may not be offset by local Fe enrichment. Further experimental, theoretical and thermodynamic analyses are required to resolve these and related issues.

Acknowledgements

We would like to thank Dave Stevenson, Kei Hirose, Taku Tsuchiya, Renata Wentzcovitch, Mark Ghiorso, Jamie Kellogg and Toshiro Tanimoto for stimulating discussions. We acknowledge support from the NSF-CSEDI, NSF-EAR and ITR programs and the DOE. The summer 2004 CIDER workshop at UC Santa Barbara KTIP was the impetus for this study.

References

Akber-Knutson, S., Neumann, G.S., Asimow, P.D., 2005. Effect of Al on the sharpness of the $MgSiO_3$ perovskite to post-perovskite phase transition. Geophys. Res. Lett. 32, L14303, doi:10.1029/2005GL023192.

Alfe, D., Gillan, M.J., Vočadlo, L., Brodholt, J., Price, G.D., 2002. The *ab initio* simulation of the Earth's core. Phil. Trans. R. Soc. Lond. 360, 1224–1227.

Badro, J., Fiquet, G., Guyot, J., Rueff, J.P., Struzhkin, V.V., Vanko, G., Monaco, G., 2003. Iron partitioning in earth's mantle: toward a lower mantle discontinuity. Science 300, 789–791.

Badro, J., Rueff, J.P., Vanko, G., Monaco, G., Fiquet, G., Guiyot, F., 2004. Electronic transition in perovskite: possible nonconvecting layers in the lower mantle. Science 305, 383–386.

Boehler, R., 2000. High-pressure experiments and the phase diagram of lower mantle and core materials. Rev. Geophys. 38, 221–245.

Boyet, M., Carlson, R.W., 2005. ^{142}Nd evidence for early (>4.53 Ga) global differentiation of the silicate earth. Science 309, 576–581.

Brana, L., Helffrich, G., 2004. A scattering region near the core-mantle boundary under the North Atlantic. Geophys. J. Int. 158, 625–636.

Brodholt, J.P., Dobson, D.P., 2005. Subducted banded iron formations as a source of ultralow-velocity zones at the core-mantle boundary. Nature 434, 371–374.

Brunet, D., Yuen, D.A., 2000. Mantle plumes pinched in the transition zone. Earth Planet. Sci. Lett. 178, 13–27.

Dziewonski, A.M., Anderson, D.L., 1981. Preliminary Reference Earth Model (PREM). Phys. Earth Planet. Inter. 25, 297–356.

Earle, P.S., Shearer, P.M., 1997. Observations of PKKP precursors used to estimate small-scale topography on the core-mantle boundary. Science 277, 667–670.

Garnero, E.J., Maupin, V., Lay, T., Fouch, M.J., 2004. Variable azimuthal anisotropy in Earth's lowermost mantle. Science 306, 259–261.

Grand, S.P., van der Hilst, R.D., Widiyantoro, S., 1997. High resolution global tomography: a snapshot of convection in the Earth. Geol. Soc. Am. Today 7, 1–7.

Hansen, U., Yuen, D.A., 1988. Numerical simulations of thermal-chemical instabilities at the core-mantle boundary. Nature 334, 237–240.

Hedlin, M., Shearer, P.M., 2002. Probing mid-mantle heterogeneity using PKP coda waves. Phys. Earth Planet. Inter. 130, 195–208.

Hedlin, M.A.H., Shearer, P.M., Earle, P.S., 1997. Seismic evidence for small-scale heterogeneity throughout the Earth's mantle. Nature 387, 145–150.

Helmberger, D.V., Wen, L., Ding, X., 1998. Seismic evidence that the source of the Iceland hotspot lies at the core-mantle boundary. Nature 396, 251–255.

Hernlund, J., Thomas, C., Tackley, P.J., 2005. A doubling of the post-perovskite phase boundary and structure of the Earth's lowermost mantle. Nature 434, 882–886.

Hirose, K., Karato, S., Cormier, V., Brodholt, J., Yuen, D., 2006. Unsolved Problems in the lowermost Mantle. Geophys. Res. Lett. 33, L12S01, doi:10.1029/2006GL025691.

Hirose, K. Post-Perovskite phase transition and its geophysical implications. Rev. of Geophys. 44(3), RG3001, doi:10.1029/2005RG000186.

Iitaka, T., Hirose, K., Kawamura, K., Murakami, M., 2004. The elasticity of the MgSiO3 post-perovskite phase in the Earth's lowermost mantle. Nature 430, 442–445.

Ishii, M., Tromp, J., 1999. Normal-mode and free-air gravity constraints on lateral variations in velocity and density of Earth's mantle. Science 285, 1231–1236.

Jeanloz, R., Knittle, E., 1989. Density and composition of the lower mantle. Phil. Trans. Roy. Soc. Lond. 328, 377–389.

Jellinek, A.M., Manga, M., 2004. Links between long-lived hot spots, mantle plumes, D″ and plate tectonics. Rev. Geophys. 42, 1–35.

Kellogg, L.H., Hager, B.H., van der Hilst, R.D., 1999. Compositional stratification in the deep mantle. Science 282, 1881–1884.

Kennett, B.L.N., 1998. On the density distribution within the Earth. Geophys. J. Int. 132, 374–382.

Lay, T., Garnero, E., Williams, Q., 2004. Partial melting in a thermal-chemical boundary layer at the base of the mantle. Phys. Earth Planet. Inter. 146, 441–467.

Mao, W.L., Shen, G., Prakapenka, V.B., Meng, Y., Campbell, A.J., Heinz, D.L., Shu, J., Hemley, R.J., Mao, H., 2004. Ferromagnesian postperovskite silicates in the D″ layer. PNAS 45, 15867–15869.

Mao, W.L., Mao, H.K., Sturhahn, W., Zhao, J., Prakapenka, V.B., Meng, Y., Shu, J., Fei, Y., Hemley, R.J., 2006. Iron-rich post-perovskite and the origin of ultralow-velocity zones. Science 312, 564–565.

Matyska, C., Yuen, D.A., 2005. The importance of radiative heat transfer on superplumes in the lower mantle with the new post-perovskite phase change. Earth Planet. Sci. Lett. 234, 71–81.

Murakami, M., Hirose, K., Sata, N., Ohishi, Y., 2005. Post-perovskite phase transition and mineral chemistry in the pyrolitic lowermost mantle. Geophys. Res. Lett. 32, doi:10.1029/2004GL021956.

Murakami, M., Hirose, K., Sata, N., Ohishi, Y., Kawamura, K., 2004. Phase transition of $MgSiO_3$ perovskite in the deep lower mantle. Science 304, 855–858.

Nakagawa, T., Tackley, P.J., 2004. Effects of perovskite-post-perovskite phase change near core-mantle boundary in compressible mantle convection. Geophys. Res. Lett. 31, doi:10.1029/2004GL020648.

Nakagawa, T., Tackley, P.J., 2006. Three-dimensional structures and dynamics in the deep mantle: effects of post-perovskite phase change and deep mantle layering. Geophys. Res. Lett. 33, L12S11, doi:10.1029/2006GL025719.

Navrotsky, A., 1994. Physics and Chemistry of Earth Materials. Cambridge University Press, chapter 7.

Nolet, G., Karato, S., Montelli, R., 2006. Plume fluxes from seismic tomography: a Bayesian approach. Earth Planet. Sci. Lett. 248, 685–699.

Oganov, A.R., Ono, S., 2004. Theoretical and experimental evidence for a post-perovskite phase of $MgSiO_3$ in Earth's D″ layer. Nature 430, 445–448.

Olson, P.L., Schubert, G., Anderson, C., 1987. Plume formation in the D″-layer and the roughness of the core-mantle boundary. Nature 327, 409–415.

Ono, S., Funakoshi, K., Ohishi, Y., Takahashi, E., 2005. In situ X-ray observation of the phase transformation of Fe_2O_3. J. Phys.: Condens. Matter 17, 269–276.

Pitzer, K., 1995. Thermodynamics, third ed. McGraw-Hill, Inc.

Puster, P., Jordan, T.H., 1997. How stratified is mantle convection? J. Geophys. Res. 102, 7625–7646.

Richter, F., 1973. Dynamical models for seafloor spreading. Rev. Geophys. Space Phys. 11, 223–287.

Schubert, G., Yuen, D.A., Turcotte, D., 1975. Role of phase transitions in a dynamic mantle. Geophys. J. R. Astr. Soc. 42, 705–735.

Shim, S.H., Duffy, T.S., Jeanloz, R., Shen, G., 2004. Stability and crystal structure of $MgSiO_3$ perovskite to the core-mantle boundary. Geophys. Res. Lett. 31, doi:10.1029/2004GL019639.

Sidorin, I., Gurnis, M., Helmberger, D.V., Ding, X., 1998. Interpreting D″ seismic structure using synthetic waveforms computed from dynamic models. Earth Planet. Sci. Lett. 163, 31–41.

Sidorin, I., Gurnis, M., Helmberger, D.V., Ding, X., 1999. Evidence for a ubiquitous seismic discontinuity at the base of the mantle. Science 286, 1326–1331.

Stackhouse, S., Brodholt, J.P., Price, G.D., 2005. High temperature elastic anisotropy of the perovskite and post-perovskite polymorphs of Al_2O_3. Geophys. Res. Lett. 32, doi:10.1029/2005GL023163.

Tedesco, M., Spera, F.J., 1991. Stability of a chemically layered upper mantle. Phys. Earth Planet. Inter. 71, 85–99.

Trampert, J., Deschamps, F., Resovsky, J., Yuen, D.A., 2004. Probabilistic tomography maps chemical heterogeneities throughout the lower mantle. Science 306, 853–856.

Tsuchiya, T., Tsuchiya, J., Umemoto, K., Wentzcovitch, R.M., 2004a. Phase transition in $MgSiO_3$ perovskite in the earth's lower mantle. Earth Planet. Sci. Lett. 224, 241–248.

Tsuchiya, T., Tsuchiya, J., Umemoto, K., Wentzcovitch, R.M., 2004b. Elasticity of post-perovskite $MgSiO_3$. Geophys. Res. Lett. 32, doi:10.1029/2004GL020278.

Van der Hilst, R.D., Karason, H., 1999. Compositional heterogeneity in the bottom 1000 kilometers of Earth's mantle: toward a hybrid convection model. Science 283, 1885–1888.

Van der Hilst, R.D., Widyantoro, S., Engdahl, E.R., 1997. Evidence for deep mantle circulation from global tomography. Nature 386, 578–584.

Williams, Q., Garnero, E.J., 1996. Seismic evidence for partial melt at the base of the Earth's mantle. Science 273, 1528–1530.

Yuen, D.A., Peltier, W.R., 1980. Mantle plumes and the thermal stability of the D″ layer. Geophys. Res. Lett. 7, 625–628.

Yuen, D.A., Cadek, O., Chopelas, A., Matyska, C., 1993. Geophysical inferences of thermal-chemical structures in the lower mantle. Geophys. Res. Lett. 20, 899–902.